LASER INTERFEROMETER GRAVITATIONAL WAVE OBSERVATORY
- LIGO -
CALIFORNIA INSTITUTE OF TECHNOLOGY
MASSACHUSETTS INSTITUTE OF TECHNOLOGY

Technical Note **LIGO-T1400038–v1** 2014/02/01

Intensity Stabilization of Lasers in LIGO Labs on the Caltech Campus

Charles Blakemore
Mentor: Rana Adhikari, Professor of Physics, Caltech
Co-Mentors: Nicolas Smith-Lefebvre, Postdoctoral Scholar, Caltech
Jenne Driggers, Ph.D. Student, Caltech

California Institute of Technology
LIGO Project, MS 18-34
Pasadena, CA 91125
Phone (626) 395-2129
Fax (626) 304-9834
E-mail: info@ligo.caltech.edu

Massachusetts Institute of Technology
LIGO Project, Room NW22-295
Cambridge, MA 02139
Phone (617) 253-4824
Fax (617) 253-7014
E-mail: info@ligo.mit.edu

LIGO Hanford Observatory
Route 10, Mile Marker 2
Richland, WA 99352
Phone (509) 372-8106
Fax (509) 372-8137
E-mail: info@ligo.caltech.edu

LIGO Livingston Observatory
19100 LIGO Lane
Livingston, LA 70754
Phone (225) 686-3100
Fax (225) 686-7189
E-mail: info@ligo.caltech.edu

http://www.ligo.caltech.edu/

1 Abstract

Interferometric gravitational wave detectors such as the Laser Interferometer Gravitational Wave Observatory (LIGO), are some of the most precise instruments used today, detecting gravitational strains as small as 10^{-22}. However, there are many significant sources of noise when measuring such small displacements, including fluctuations in the output power of the carrier light lasers. In an effort to reduce these fluctuations, this project aims to design and construct an Intensity Stabilization Servo (ISS), a feedback control system that reduces laser intensity noise. By comparing the unstabilized laser power spectrum to the noise spectrum set by the thermal fluctuations in the mirror coatings used on the interferometers test masses (considered a theoretical limit), it was possible to calculate an open-loop gain requirement for the servo. To meet this requirement, an analog circuit was designed and prototyped on a breadboard while its transfer function was determined using a spectrum analyzer. With the filtering behavior of the analog servo verified, the design schematics were transferred to a printed circuit board (PCB) layout. The completed board will be tested, and its behavior optimized, in both the LIGO 40m prototyping interferometer as well as other LIGO facilities on the Caltech campus

2 Introduction

One of the most significant issues limiting detection of gravitational waves at LIGO is the signal-to-noise ratio observed in most measurements. A few of the major sources of noise included thermally generated vibrations, seismic activity and mechanical vibrations, electronic noise from signal processing as well as RMS fluctuations in the intensity of the carrier light laser [1].

The efforts of a significant number of researchers have been dedicated to addressing these noise limitations. Thermal noise generated by the coatings of the test masses used in LIGO interferometers has been calculated and the coating optimized to reduce this noise [2]. Seismic isolation stacks serve to reduce mechanical vibrations of the many different optics used [3]. In aLIGO and many of the associated labs, laser intensity stabilization has also been employed to great effect [4]. Often, it is possible to reduce the noise of the laser sufficiently below other contributions.

As part of the LIGO collaboration, the 40m Lab on the Caltech campus can serve as a prototyping stage for instruments and techniques that may eventually be used in Advanced LIGO (aLIGO), the now current generation of detector being pursued. The designs for an Intensity Stabilization Servo (ISS) have been discussed at the 40m Lab, although never employed. Creating a working ISS would allow more precise measurements to be taken and thus allow for more accurate assessments of efforts to increase overall sensitivity in the 40m Lab and eventually in aLIGO.

Much work has already been done concerning intensity stabilization in general and more specifically, of the NPRO laser used in aLIGO [5]. AC-coupled ISS systems, especially ones employed at aLIGO, involve three main parts: a photodiode or photodiode array and a calibrated voltage reference to produce an error signal, a servo circuit to amplify the error

signal and finally an Acousto-Optic Modulator to feed back the error signal and adjust the power of the laser incident on the photodiode(s) (and thus adjust the effective power of the laser). The general design of the ISS will be very similar, although the noise suppression behavior of this feedback loop will depend on the desired application.

3 Objectives

The primary objective of my work was the design and construction of an ISS system to reduce the intensity noise of lasers used in the LIGO interferometer at Caltech. In addition to reducing noise at the 40m Lab, such an ISS could be included to obtain higher sensitivity in other experiments that use similar lasers, such as LIGOs Cryo Lab on the Caltech campus. As such, the ISS has been designed with a modular behavior so that it might be applied to multiple experiments/facilities.

Requirements for the noise suppression behavior of our ISS have been determined by examining significant contributions to noise as well as defining some constraints on the ISS itself. Based on these requirements, I have designed two prototype servos, one for use in the 40m Lab and another for use in the Coating Thermal Noise (CTN) Experiment.

4 Motivation

It is worthwhile to discuss, in part, the motivation for intensity stabilization. LIGO observatories operate by detecting very small differences between the lengths of two arms of an interferometer. As such, anything that changes these arm lengths has an effect on attempted measurement of gravitational waves.

We, in particular, are concerned with laser light impinging on the surface of a LIGO test mass, which causes thermal expansion of the mirror coating. The steady state expansion can be accounted for, but fluctuations in the laser light couple to fluctuations in the expansion of the mirror coating. These fluctuations can then contribute significant noise to any attempted final measurement.

We briefly reproduce some calculations and results from Cerdonio et al. [6]. The authors calculated thermodynamic noise, photo-thermal noise and the noise due to fluctuating radiation pressure on the mirrors. Thermodynamic noise is generated through statistical fluctuations and the resulting dissipation while photo-thermal and radiation pressure noise are due to impinging laser light.

It was found that the radiation pressure noise was significantly higher than the photo-thermal noise with a choice of reasonable parameters of the optical cavity in question. Thus we only concern ourselves with the results of the radiation pressure analysis. Starting from first principles, Cerdonio et al. state that the displacement in a mirror due to an intracavity photon flux of $N[\omega]$

$$\hat{u}[\omega] = \chi_{eff}[\omega] P_{rad}[\omega] = 2\hbar k \chi_{eff}[\omega] N[\omega]$$

Where χ_{eff} is some effective mechanical susceptibility in response to radiation pressure. From this result, the authors infer that the noise spectrum $S_{\hat{u}}[\omega]$ induced by radiation pressure is proportional to the spectral power noise $S_{cav}[\omega]$ of the intracavity light.

The authors then solve for the mechanical susceptibility χ_{eff} which they can then use to relate $S_{\hat{u}}[\omega]$ and $S_{cav}[\omega]$. The final result they reach is given by,

$$S_{\hat{u}}[\omega] = \left(\frac{2(1-\sigma^2)}{\sqrt{2\pi}Ecr_0}\right)^2 S_{cav}[\omega]$$

where E is the Young's modulus of the mirror substrate, σ is related to the stress tensor, r_0 is the beam radius incident on the mirror and c is the speed of light.

The main result to take away from this brief reproduction is simply that fluctuations in the cavity laser light can induce displacement fluctuations in the mirrors, subsequently introducing more noise into any attempted measurements. This would naïvely imply that intensity stabilization of lasers is well-motivated. With this in mind, we proceed to discussing the intensity stabilization system designed herein.

5 Approach

In general terms we proceeded as follows,

1. Determined various noise requirements and device limitations.
2. Based on these requirements and currently observed noise, formalized desired feedback behavior of the ISS.
3. Using programs such as LISO and Matlab, simulated proposed ISS designs.
4. A prototype servo circuit was designed on a breadboard and characterized to affirm the aforementioned behavior.
5. With a successful prototype, the ISS was built on PCB and is now being tested and characterized.
6. If necessary, the filtering behavior of the ISS can be modified to optimize performance once initial tests have been completed.

6 CTN Experiment Control System

The following block diagram, Figure 1 displays a very general control system. We have some input signal 'x' and an output 'y'. There is a single feedback path with gain G that sums with the input signal. More complicated control systems can have additional components with different gain/throughput, as we will see.

The total output is then given by

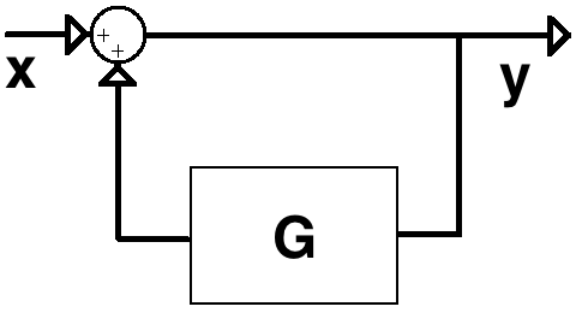

Figure 1: A general control system with open-loop gain G is shown. 'x' is the input signal and 'y' is the output signal. A simple signal analysis yields the expression y = x + Gy

$$y = x + Gy \qquad \Longrightarrow \qquad y = \frac{1}{1-G} \cdot x$$

Which is the usual expression for closed-loop gain, with open-loop gain G. We can apply a similar analysis to a block diagram of the ISS to be used in the CTN experiment.

Figure 2 shows the layout of the CTN experiment with an active ISS. Understanding that signal pathway, as well as having quantitative measurements of the behavior of each device shown, is crucial to developing an accurate requirement.

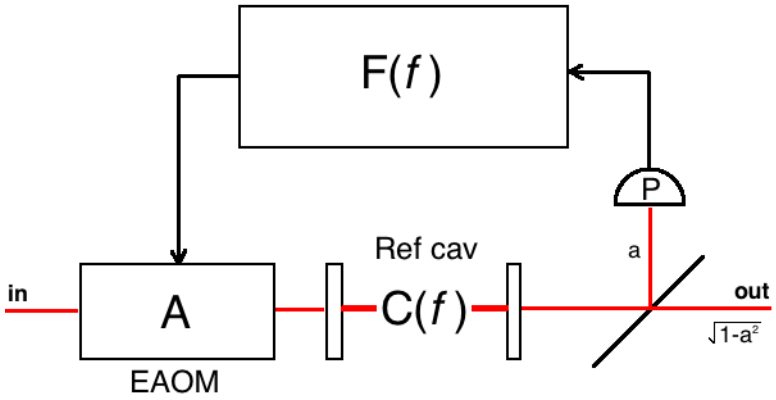

Figure 2: A simple block diagram of the ISS for the CTN experiment. To reiterate: P = photodiode gain, F(f) = servo TF, A = modulator gain, C(f) = cavity TF, a = optical throughput from beam splitter

Below, we include explicit expressions for the transfer functions of various optics and electronics included, courtesy of those working on the CTN experiment. We have 4 main devices: the reference cavity itself, a beam splitter to obtain a control signal for modulation, a photodiode to convert our optical signal into an electronic signal and an Electronic Acousto-Optic Modulator to apply the amplified control signal.

$$a = 0.5\,W/W \qquad P = 0.9 \cdot 10^4\,V/W \qquad A = 5.2 \cdot 10^{-6}\,W/V$$

$$C(f) = \left|\frac{0.6}{1+i(f/f_c)}\right| \qquad f_c = \frac{c\,T}{8\,\pi\,L} = 97\,kHz$$

The open-loop gain can be acquired fairly easily and is given by,

$$G = a\,C(f)\,P\,F(f)\,A$$

On occasion, we will also refer to the 'plant transfer function' which includes all of the optics and electronics *except* the servo board itself. This is given by the expression,

$$\text{Plant} = a\,C(f)\,P\,A \approx 0.014\,V/V$$

Where we have ignored the cavity pole at 97 kHz as our servo will have an open-loop gain less than unity at this frequency. Recognizing that the output signal is also attenuated by $C(f)$ and $\sqrt{1-a^2}$, the total closed-loop transfer function of the system in Figure 2 is given by the following:

$$\Longrightarrow\ ASD_{out} = \frac{C(f)\,\sqrt{1-a^2}}{1-C(f)\cdot a\,P\,F(f)\,A}\cdot ASD_{in} = \frac{C(f)\,\sqrt{1-a^2}}{1-G}\cdot\ ASD_{in}$$

where Amplitude Spectral Densities are in units of $\mathrm{W}/\sqrt{Hz}$ and refer to the laser's noise. The above formula essentially represents the functioning behavior of the ISS. The exact transfer function of the servo being designed, represented by block F(f), depends on two things: the plant transfer function given by the above expressions, as well as the noise suppression requirement.

7 Developing a Requirement for the CTN Experiment

7.1 Observed Noise vs. Desired Noise

Essentially two things are necessary to develop an explicit requirement for a noise suppression control system: the current amplitude spectral density (ASD) of the free-running system and the desired ASD. As this work does not directly pertain to what is done in the CTN experiment, the observed ASD and the desired ASD have been measured and formulated, respectively, by a colleague.

From the above data, as well as the plant transfer function quantified earlier, one can easily determine the necessary filtering behavior of the main servo. Ideally, we would want to suppress the free-running laser noise to a level approximately 10 times (referred to as a safety factor) lower that the theoretical brownian noise limit from the mirror coatings. Briefly,

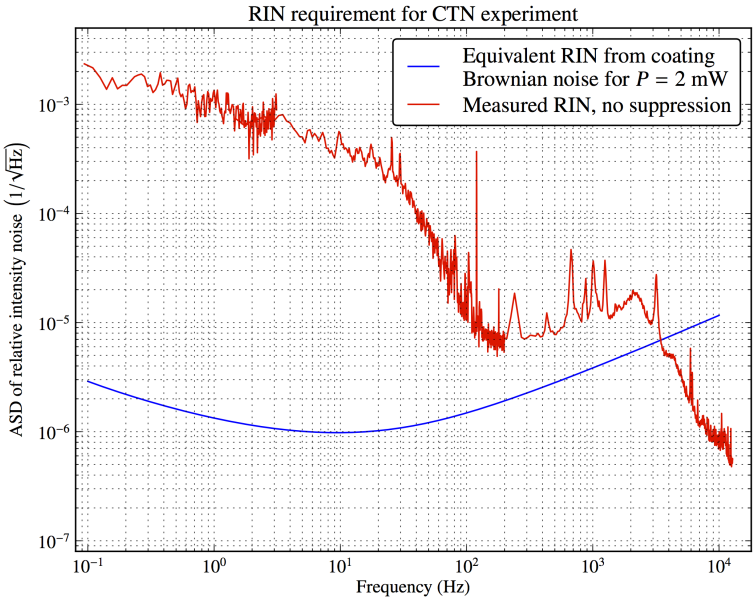

Figure 3: The spectral density of both the free-running laser as well as a theoretical noise limit manifested by the brownian noise from mirror coatings.

$$\text{Loop Noise Suppression Requirement} \approx \frac{\text{Noise Limit}}{\text{Free-running RIN}} \cdot \frac{1}{10}$$

From this requirement, we can infer the necessary open-loop transfer function of our servo board. This was done through a somewhat iterative process. A servo with open-loop gain $F(f)$ was designed such that the shape of the closed loop TF was similar to the loop suppression requirement.

$$\frac{\text{Noise Limit}}{\text{Free-running RIN}} \cdot \frac{1}{10} \approx \frac{1}{1 - F(f) \cdot \text{Plant}}$$

The shape and magnitude of $F(f)$ was tweaked until the implied closed-loop TF matched or surpassed the noise suppression requirement over our frequency range of interest.

7.2 Proposed Design

Understanding our device limitations as well as the desired behavior, a simple servo has developed. It consists of three filtering stages that can switch on in a staggered manner (this will be explained/discussed in the ISS Subsystems section). The filter stages themselves consist of an op-amp in a negative feedback configuration with some collection of resistors and capacitors in the feedback path.

The exact topology and component values of the resistors and capacitors were carefully chosen to create the desired behavior. Each stage was simulated and tuned multiple times using LISO, a analog circuit simulator, until the correct filter shape was obtained, as shown in Figure 5.

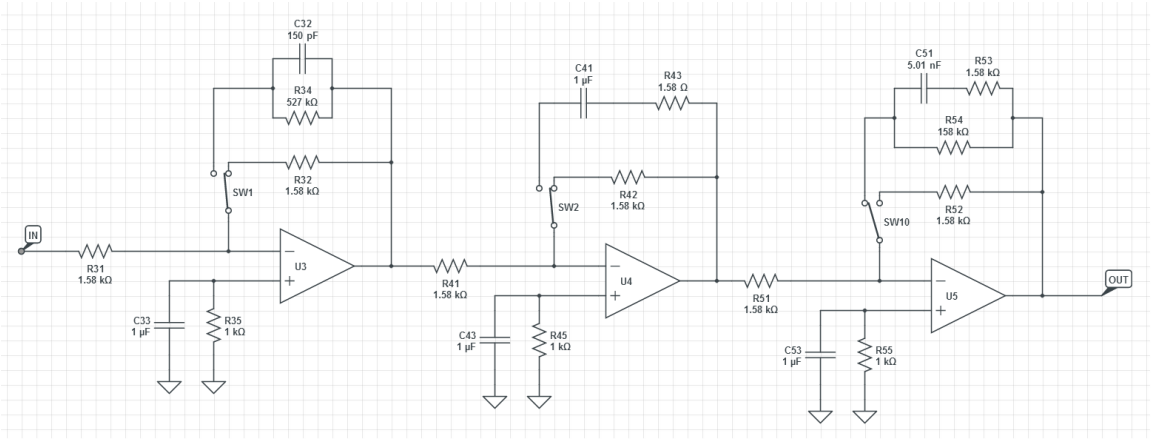

Figure 4: Proposed servo topology. The second and third stage are shown with the SPDT switches that will be used to switch from a unity-gain buffer to the more complex filter shape. Again, this mechanism will be discussed in a future section

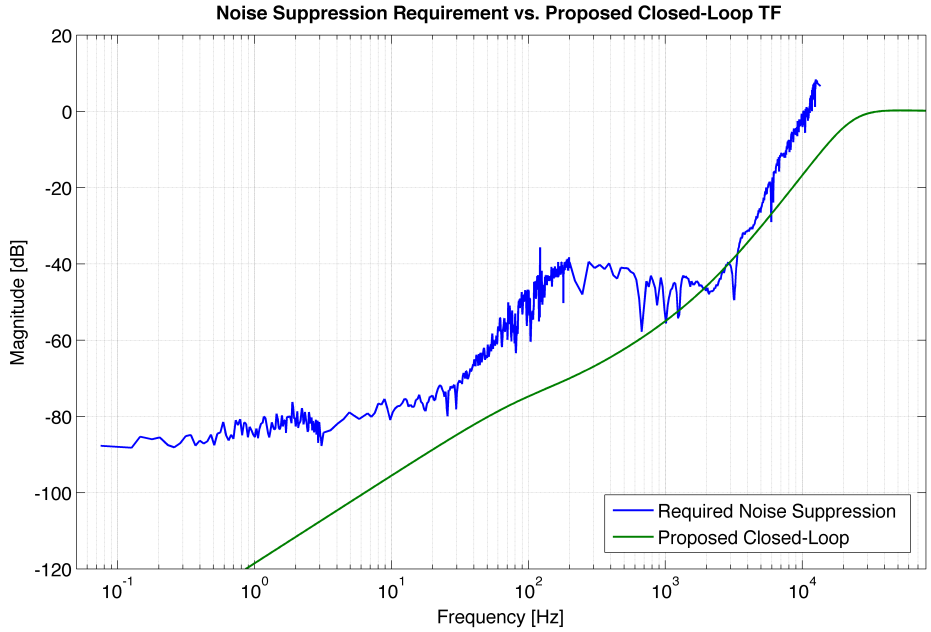

Figure 5: Desired suppression behavior (blue) and the closed-loop transfer function of the proposed servo shown in figure 3 (green). The blue curve is given explicitly by: (Noise Limit/Free-running RIN) $\cdot \frac{1}{10}$. We can see that our servo meets the requirement quite well.

With the main filtering servo design complete, we can now focus on some of the other components of the ISS.

8 ISS Subsystems

Significant time has been spent developing a detailed schematic for the full ISS system, which includes many subsystems aside from the main filtering servo. As such, a brief explanation of the purpose and design of each of the subsystems is included below. They are ordered according to their location in the signal path.

For each of the subsystems listed below, refer to the attached schematic for the relevant circuit topology.

8.1 Instrumentation Amplifier: Schematic Appendix Pg. 2

The electronics in the ISS and the photodiode which receives the input signal for the ISS are not referenced to the same ground so it is necessary to handle a differential signal. In general, a single instrumentation amplifier integrated circuit (IC) is sufficient, although one can design more complicated topologies for ulterior signal processing.

The instrumentation amplifier setup used can provide both signal gain and common mode rejection. The first is useful as photodiodes don't provide a standard voltage while we would like to be able to reference the photodiode signal to a precision 5 Volt DC reference. For instance, in the CTN experiment, colleagues are working with a 1.5 V signal (+ noise) so we would like the instrumentation amplifier to provide a gain of 3.3.

Common mode rejection suppresses such things as 60 Hz wall power noise. With the particular topology used, the Common Mode Rejection Ratio (CMRR = differential gain / common mode gain) is entirely determined by the signal gain, which is inherently differential. Since common mode signals are not a dominant source of noise, any amount of CMRR is useful, but a large CMRR is not explicitly necessary.

8.2 Dewhitening Filter: Schematic Appendix Pg. 2

Some photodiodes have very simple whitening to raise the signal and reduce noise. A typical whitening filter has the following characteristics: a zero at 1 Hz, a pole at 100 Hz and 0 dB gain at DC.

For accurate signal feedback it is then necessary to apply a dewhitening filter to raise the low frequency signals. The aforementioned whitening filter would have a dewhitening counterpart with a pole at 1 Hz, a zero at 100 Hz and 0 dB gain at 10kHz. In the ISS schematic, the dewhitening filter can be bypassed with a jumper if the photodiode used does not have whitening.

8.3 Differential/Summing Amplifier: Schematic Appendix Pg. 2

To obtain the error signal for amplification and subsequent feedback, one can reference the photodiode signal to a fixed DC voltage. This is usually done with a differential amplifier which outputs the difference between two input voltages. In the early versions of the ISS

design, it was assumed that the signal from the photodiode would be a positive voltage, but this is not always the case.

To account for this, I have included two signal paths (only one of which will be used at a time): one path makes use of an op-amp in a differential amplifier configuration while the other uses an op-amp in a summing amplifier configuration, in case the photodiode voltage is negative.

8.4 Input Grounding and Inverting Amplifier: Schematic Appendix Pg. 2

These two systems will be operated with front panel switches.

For characterization and debugging, it is useful to ground the ISS input so a zero-amplitude signal is sent through the filtering servo and other subsystems. By connecting the input terminals of the differential/summing amplifier, one can effectively ground the input.

In feedback systems, it is common to have the feedback signal inverted (an extraneous '-1' in the gain). As such, it is useful to have an amplifier that can provide a programmable gain of ± 1. This is done with a simple SPDT switch and an op-amp.

8.5 Comparator and Boost Switching: Schematic Appendix Pg. 4

When initializing an analog control system, such as the one discussed here, the actuator that reapplies the error signal for noise suppression can be saturated. Operating at saturation usually has negative consequences and can destabilize the entire servo. To avoid this, a system has been designed that initializes the noise suppression filters in stages.

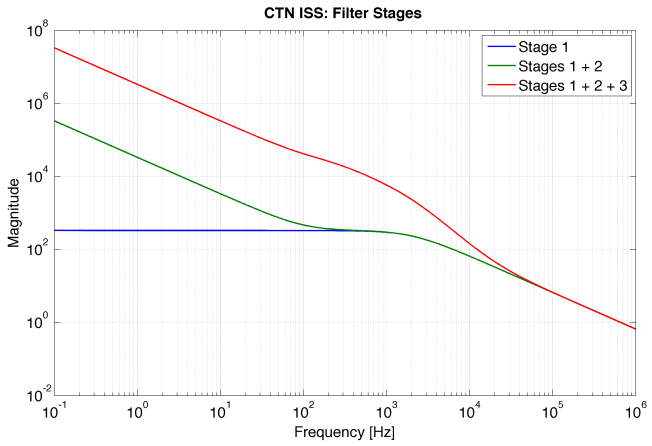

Figure 6: Shown is the magnitude of the transfer function of the servo as successive boosts turn on. Blue: 1st stage. Green: 1st+2nd stage. Red: Full servo.

The filter servo is composed of three stages, as discussed before. The first stage is a LP filter and is always turned on. Essentially this means that any error signal that passes through the ISS will be low-pass filtered. This first stage thus applies some amount of noise suppression when the ISS loop is closed.

Initially, the second and third stage, referred to as boosts, are in a unity gain configuration and act as simple voltage followers. A secondary system monitors the noise suppression of the first stage and 'turns on' the second and third stage when the RMS noise of the error signal has dropped below a certain threshold.

To do this, the error signal input to the filtering servo is taken down another signal path which first amplifies the signal then passes it through an RMS-to-DC converter chip. This chip takes an AC input, our amplified error signal, and outputs a DC voltage equivalent to the RMS value of the AC input. The DC output is then fed into one input of a comparator which compares it to a user defined threshold between 1 and 4 Volts and acts as a Schmitt trigger. A Schmitt trigger compares two inputs and has two discrete outputs: one high and one low. In this case, the high and low output of the Schmitt trigger are used as logic to switch on the second and third stages.

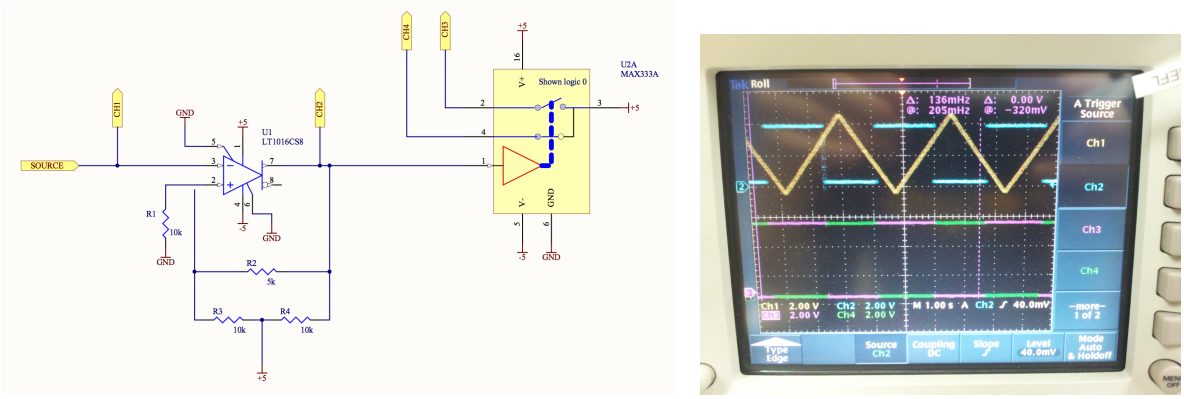

Figure 7: (a) Topology of one proposed comparator. Ports are included which represent the oscilloscope channels used in the accompanying image (b) Shown is an image of the comparator operating as desired. The yellow trace represents a varying input and the blue represents the output of the comparator. This square-wave-like signal is then used to drive the logic input of a SPDT switch

Understanding the signal path, we can consider how this subsystem operates. As the first stage of the ISS suppresses noise, the RMS value of the error should theoretically decrease. This, in turn, should result in a decreasing DC voltage applied to one input of the comparator. Initially, the comparator will be be in its low-level output configuration which corresponds to the DC output from the RMS-to-DC converter being larger than the defined threshold. As the DC level drops below the threshold with continued noise reduction from the first stage, the comparator switches to its high-level output.

The high-level output is then used to switch the second and third boost from their unity gain configuration to their more complicated filtering configuration (using the same type of switching behavior as detailed above in figure 5). The high-level output is first passed through LP filters with large time constants that act as analog delays so that the initialization of the boosts can be staggered. A time constant of 1 second delays the second stage from initializing after the comparator switches while a time constant of 5 seconds delays the third stage from initializing. This is all done in an effort to prevent saturation of the actuator.

8.6 Excitation: Schematic Appendix Pg. 5

This subsystem has one simple goal: facilitate measuring the open-loop transfer function of the ISS with the loop closed. This can be used both as an initial diagnostic tool as well as during operation of the ISS. A differential driver takes some input (for measuring a transfer function, this will be a sine of varying frequency) and adds it to the signal path while two voltage followers monitor the voltage directly before and after the excitation input. And thus one obtains the closed-loop TF.

9 Completed PCB and Initial Board Characterization

The PCB layout in Schematic Appendix Pg. 6 was submitted to Sunstone PCBexpress. Components were soldered on the board promptly after it was received. The completed PCB, both bare and with all the components, is shown below.

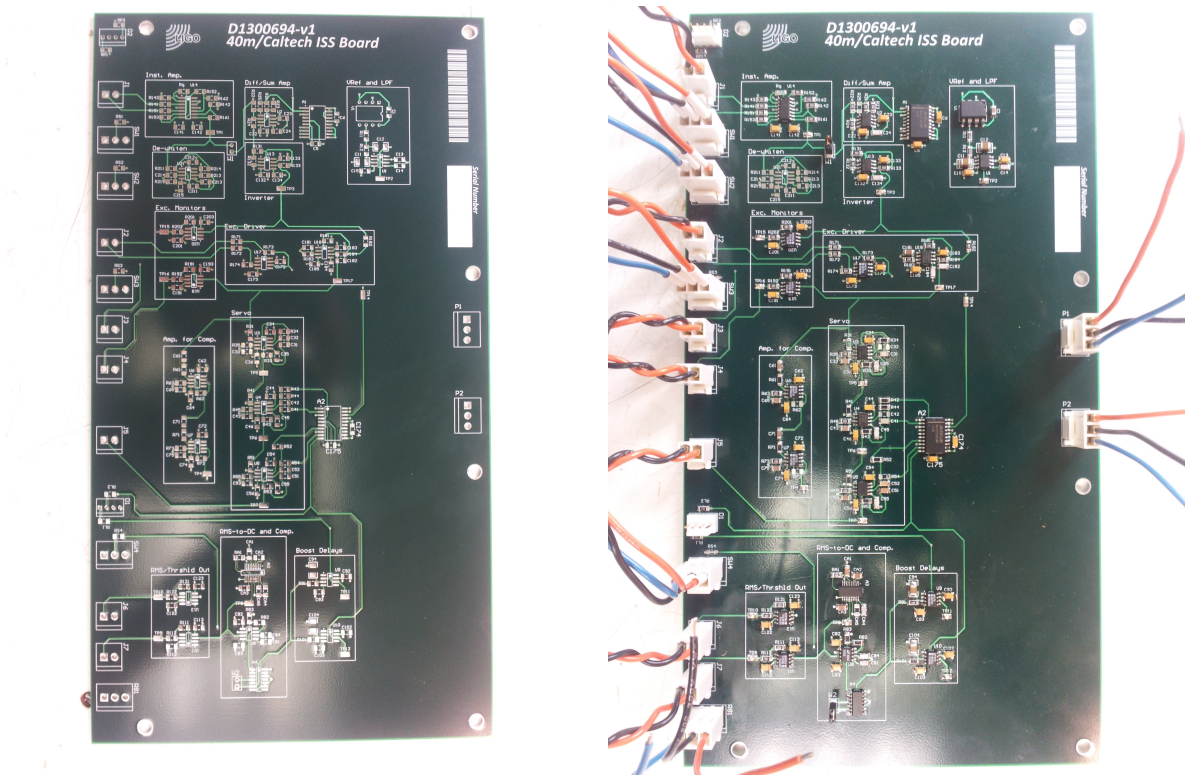

Figure 8: (left) Empty PCB board as received from manufacturer (right) Board stuffed with all components and with attached/wired headers.

Based on initial continuity tests, the board seemed to be functioning correctly. Power was correctly distributed to all components and ground was established in all locations that were checked.

The next stage of characterization was the attempted measuring of the servo's transfer function. Because the servo has such high gain (10^6 near 1 Hz), it is impractical to measure

the open loop transfer function directly. However, one can 'close the loop' by connecting the output of the board to the input. This was done with a 36 dB attenuator to simulate the plant transfer function.

Using the Excitation feature of the board, the open- and closed-loop transfer functions were measured. In each case, the transfer function was measured both with the boosts on and with the boosts off.

9.1 Open-Loop Transfer Function

An SR785 was used to drive the excitation input and measure the open-loop transfer function, Figure 9 below. This was done using the excitation monitors discussed in the Subsystems section.

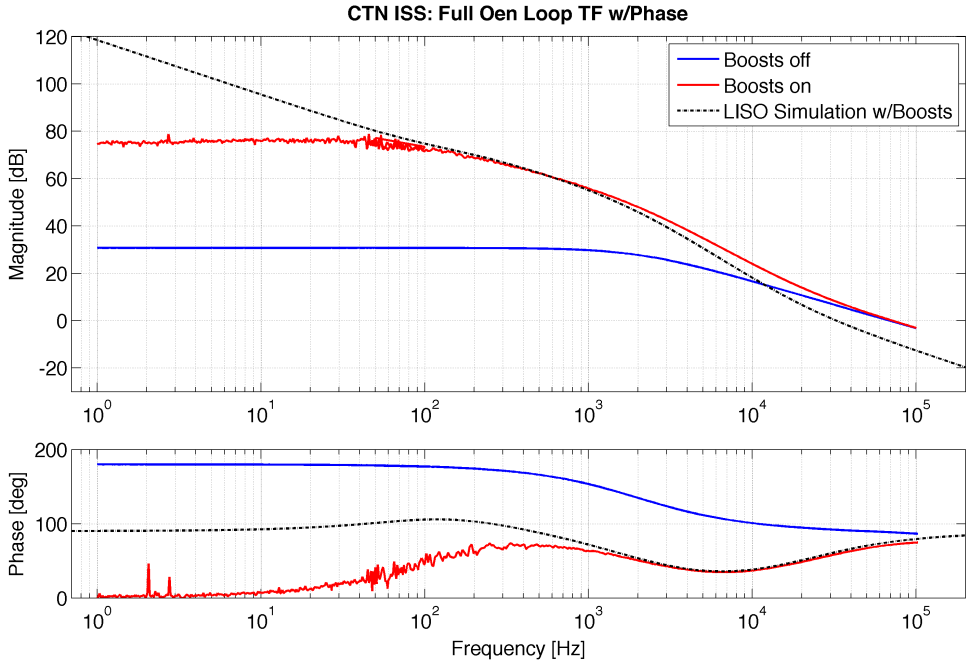

Figure 9: Open-loop transfer function of the servo board with a 36 dB attenuator simulating plant electronics/optics. With boosts off, we see low-pass filter behavior which matches simulation quite well. With boosts engaged, our TF is limited by op-amp railing for low frequency, although it is fairly consistent otherwise. Note the phase matching introduced at low frequency due to op-amp railing.

First note that based on LISO simulations, this loop is unconditionally stable as the unstable unity gain crossing would be at 0 degrees and we can see that the phase stays well above 0 degrees over the working frequency range of this device.

At low frequency, we can see that the transfer function reaches a maximum magnitude, which is simply a result of the op-amps railing in response to the relatively large excitation input from the SR785. *In situ*, the 'input' will be a much smaller signal and thus not cause the same railing.

The slightly shifted unity gain frequency as compared to simulation simply results from use of components with somewhat large tolerances. In later versions, more accurate components will be used to prevent the shifting of various corner frequencies.

9.2 Closed-Loop Transfer Function

Similarly, one can measure the closed-loop transfer function, Figure 10, using the SR785 to drive the excitation. We then analyze one of the monitor signals and the driving signal to obtain $1/(1-G)$ as the location of one of the excitation monitors allows for direct measuring of the signal: $\text{in} \cdot (1-G)$.

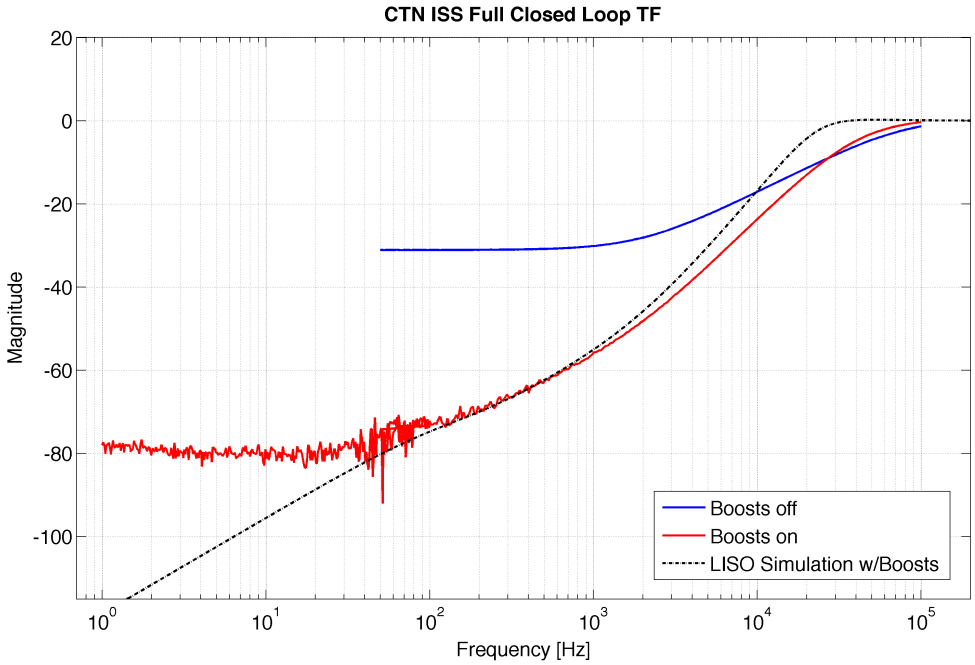

Figure 10: Closed-loop transfer function of the servo board with a 36 dB attenuator simulating plant electronics/optics. Note that low-frequency data for the servo state with the boosts off is not included here due to negligence. As with the open-loop TF, we can see that at low frequency in the boost-on state, the op-amps begin saturating resulting in a flattening of the transfer function. However, the measured transfer function for $f > 100Hz$ is consistent with simulation.

Just as before, the unity gain frequency (and thus where the closed-loop TF approaches 1 asymptotically) has been shifted due to components with large tolerances that skew the value of various corner frequencies. Despite this, our servo meets the noise suppression requirements quite well.

The above plot suggests that once other minor issues (discussed later in Debugging section) are solved, we could attempt to operate the servo *in situ*, as our board is behaving almost exactly as expected.

9.3 Closed-Loop Transfer Function vs Requirement

Just as a check, we plot our measured transfer function against the closed-loop requirement which includes a safety factor.

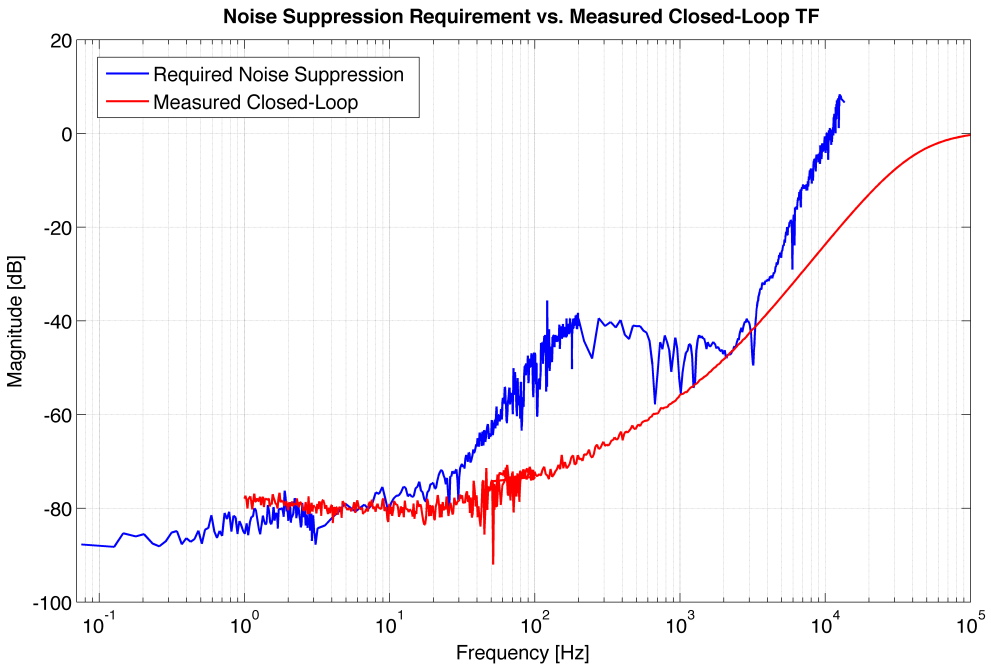

Figure 11: Closed-loop transfer function of the servo board with a 36 dB attenuator simulating plant electronics/optics. This is plotted against the requirement determined earlier. We can see the servo meets the noise suppression requirement until the op-amps start railing.

10 Debugging

A few other problems concerning the functionality of the full board have been identified. These issues have not yet been resolved but are actively being investigated.

1. The 5V reference is not actually producing 5V, more like 2.9V

   Use of a FET op-amp for the buffer will most likely resolve this issue

2. The AD8436 is causing significant fluctuation in the -5 V power line.

   A simple circuit using only this part was designed and the same issue is not observed. IT's possible that a particular chip was causing this problem, although it's currently unknown.

3. The method used to ground the input mistakenly passes a high current through one of the Quad SPDT switches, causing chip failure

These problems will be addressed as soon as possible.

References

[1] Sigg, D. (for the LIGO Scientific Collaboration). *Status of the LIGO detectors*. Class. Quantum Grav. **25**, 114041 (2008).

[2] Castaldi, G.; Galdi, V.; Pierro, V.; Pinto, I. M.; de Salvo, R.; Agresti, J. *Coating Design Optimization for Advanced Interferometers: Minimizing the Total Noise Budget*. LSC-Virgo Joint Meeting, Cascina, Pisa, Italy, May 2007.

[3] Abbot, R.; Adhikari, R.; Allen, G.; Cowley, S.; Daw, E.; DeBra, D.; Giaime, J.; Hammond, G.; Hammond, M.; Hardman, C.; How, J.; Hua, W.; Johnson, W.; Lantz, B.; Mason, K.; Mittleman, R.; Nichol, J.; Richman, S.; Rollins, J.; Shoemaker, D.; Stapfer, G.; Stebbins, R. *Seismic isolation for Advanced LIGO*. Class. Quantum Grav. **19**, 1519 (2002).

[4] Krämer, C.; Pold, J. H.; Kwee, P.; Kim, H.; Willke, B.; Danzmann, K. *Stabilization of the Advanced LIGO laser*. LSC-Virgo Joint Meeting, Arcadia, California, USA, Mar 2010.

[5] Kwee, P.; Bogan, C.; Danzmann, K.; Frede, M.; Kim, H.; King, P.; Pold, J.; Puncken, O.; Savage, R. L.; Seifert, F.; Wessels, P.; Winkelmann, L.; Willke, B. *Stabilized high-power laser system for the gravitational wave detector Advanced LIGO*. Opt Express **20**, 10617 (2012).

[6] Cerdonio, M.; Conti, L.; Heidmann, A.; Pinard, M. *Thermoelastic effects at low temperatures and quantum limits in displacement measurements*. Phys. Rev. **63**, 82003 (2001).

[7] Rollins, J. *Intensity Stabilization of a solid-state laser for interferometric gravitational wave detectors*. MIT Theses - Dept. of Physics, MIT 2004.

[8] Evans, M.; Ballmer, S.; Fejer, M.; Fritschel, P.; Harry, G.; Ogin, G.; *Thermo-optic noise in coated mirrors for high-precision optical mesasurments* arXiv.org

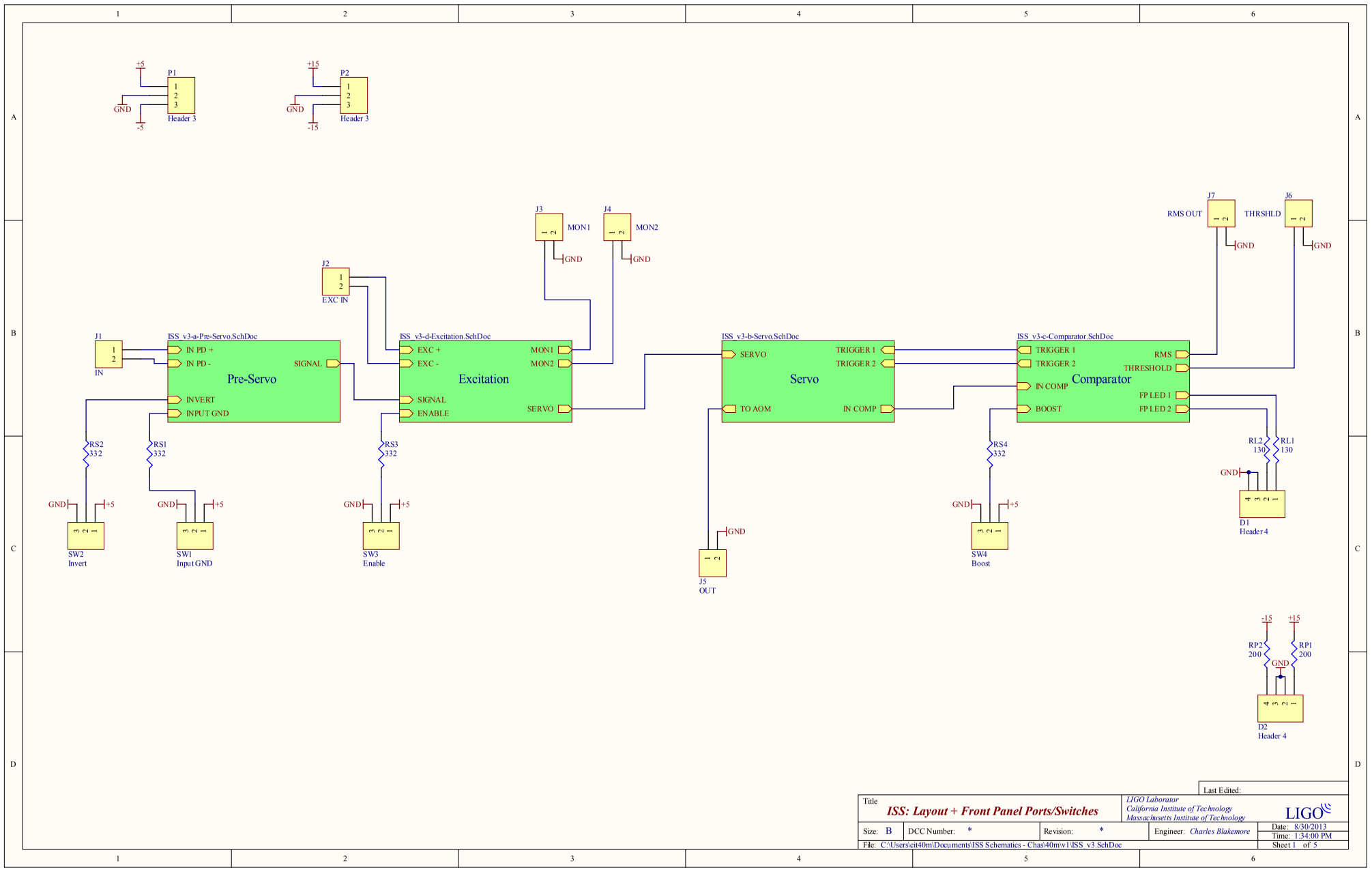

Title: *ISS: Layout + Front Panel Ports/Switches*			*LIGO Laboratory* *California Institute of Technology* *Massachusetts Institute of Technology*	LIGO
Size: B	DCC Number: *	Revision: *	Engineer: *Charles Blakemore*	Last Edited: Date: 8/30/2013 Time: 1:34:00 PM Sheet 1 of 5
File: C:\Users\cit40m\Documents\ISS Schematics - Chas\40m\v1\ISS_v3.SchDoc				

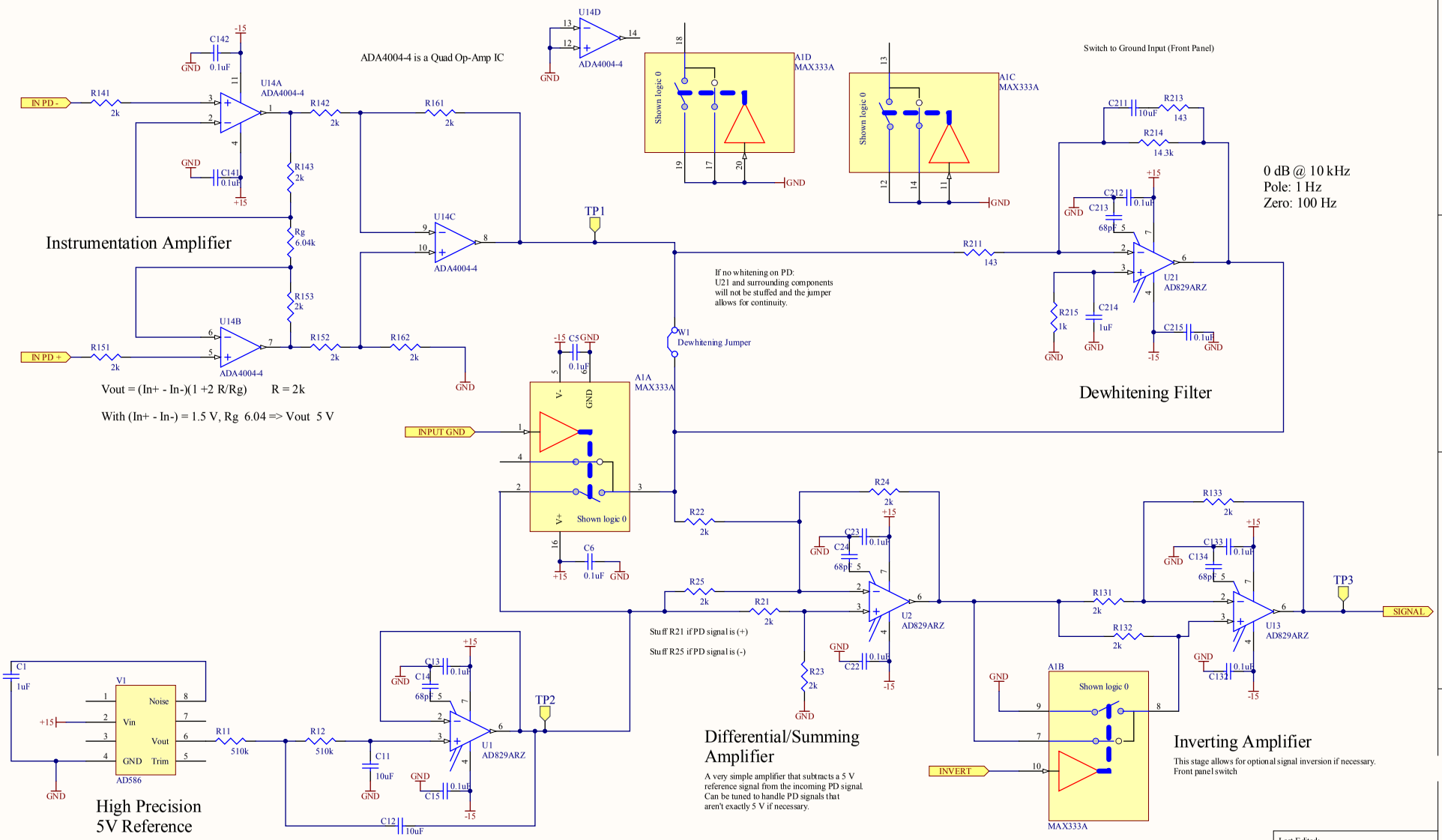

Title: *ISS: Pre-Servo*			*LIGO Laboratory* *California Institute of Technology* *Massachusetts Institute of Technology*	LIGO
Size: B	DCC Number: *	Revision: *	Engineer: *Charles Blakemore*	Date: 8/30/2013
File: C:\Users\cit40m\Documents\ISS Schematics - Chas\40m\v1\ISS_v3-a-Pre-Servo.SchDoc				Time: 1:34:00 PM
Last Edited:				Sheet 2 of 5

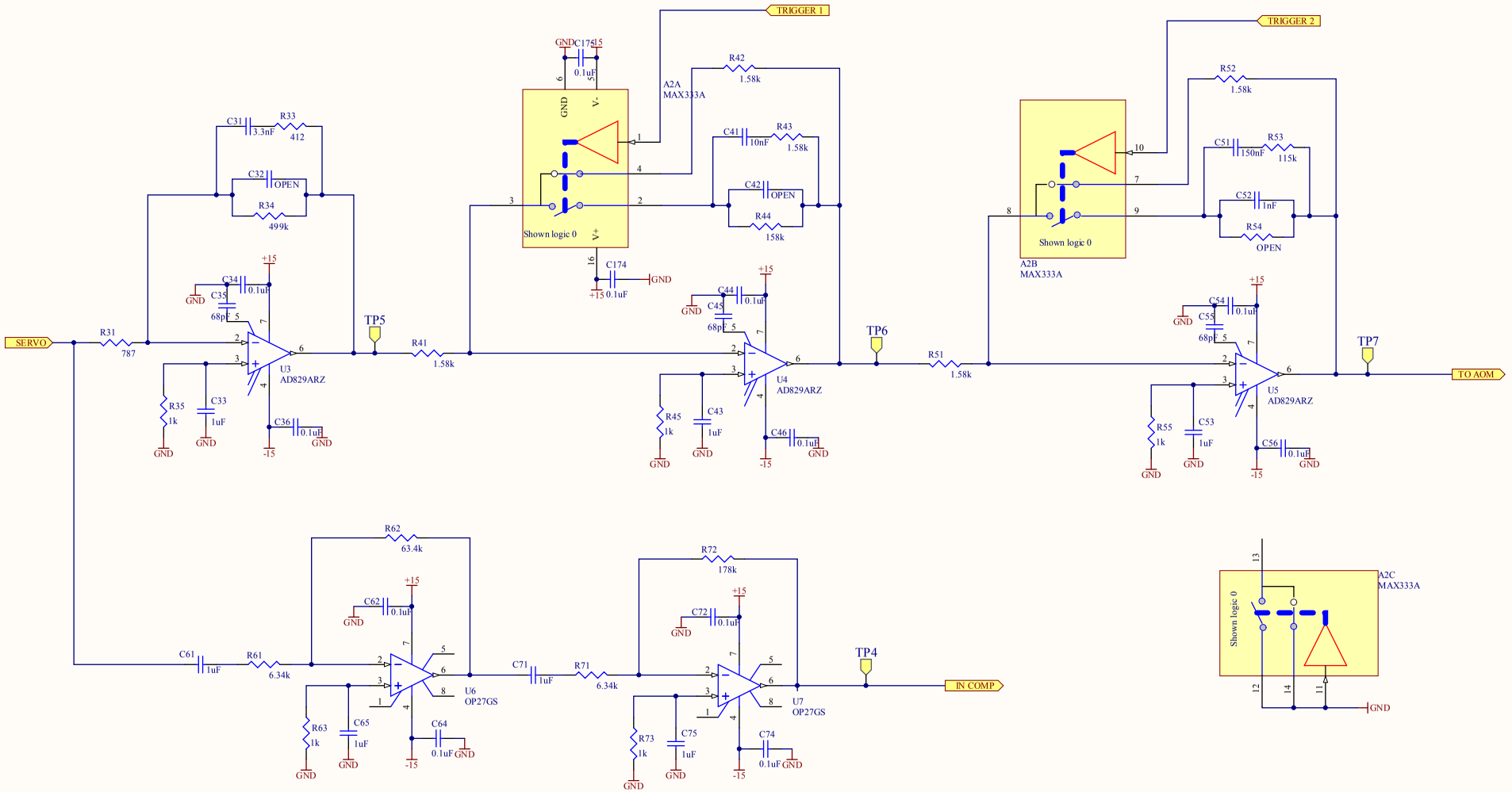

Title: *ISS: Servo*			*LIGO Laboratory* *California Institute of Technology* *Massachusetts Institute of Technology*	Last Edited:
Size: B	DCC Number: *	Revision: *	Engineer: *Charles Blakemore*	Date: 8/30/2013
File: C:\Users\cit40m\Documents\ISS Schematics - Chas\40m\v1\ISS_v3-b-Servo.SchDoc				Time: 1:34:00 PM
				Sheet 3 of 5

AD8436 RMS-to-DC Converter

Here, the AD8436 is connected according to the manufacturer reccomendations.
Pin connections on the AD8436 come directly from the manufacturer's datasheet.
(www.analog.com/static/imported-files/data_sheets/AD8436.pdf)

This is a very simple design to accomplish basic RMS-to-DC conversion
and should work quite effectively for the type of inputs we're interested in.

The LT1016 and accompanying circuitry has two states.
If the DC-voltage from the AD8436 is larger than the threshold
established by the potentiometer then the LT1016's output is
set at 0 V.

If the DC-voltage input is lower than the threshold, then the
LT1016's output is 3.5 V (based on datasheet).

The ratio R83/R82 sets the hysteresis. If Voh is the high level
output of the comp. and Vol is the low level then
deltaV (R83/R82)*(Voh - Vol)

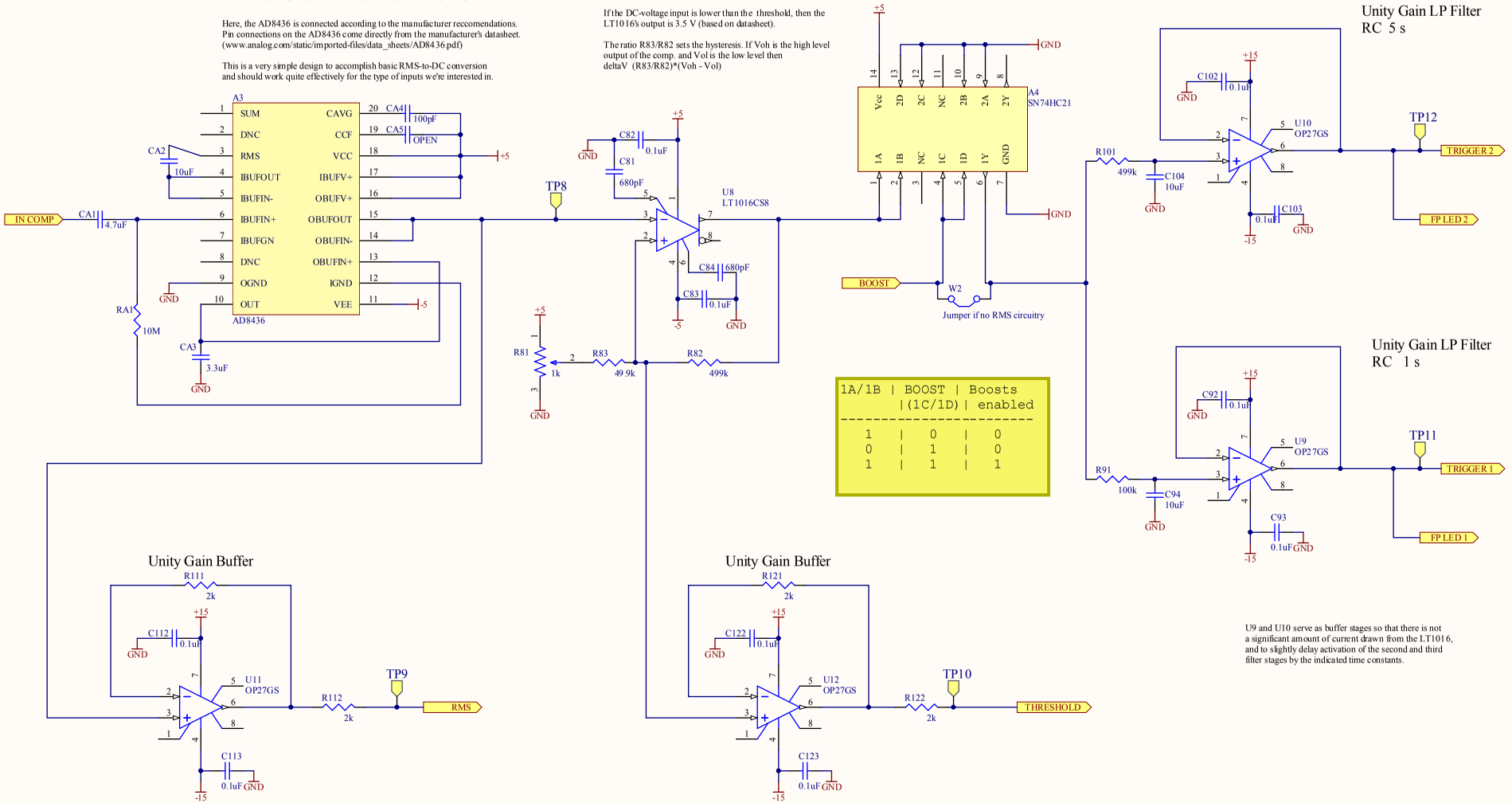

1A/1B	BOOST	Boosts |(1C/1D)| enabled
1	0	0
0	1	0
1	1	1

U9 and U10 serve as buffer stages so that there is not
a significant amount of current drawn from the LT1016,
and to slightly delay activation of the second and third
filter stages by the indicated time constants.

Last Edited:

Title: *ISS: Comparator + Triggering*	*LIGO Laboratory* *California Institute of Technology* *Massachusetts Institute of Technology*	LIGO	
Size: B	DCC Number: *	Revision: *	Engineer: *Charles Blakemore*
File: C:\Users\cit40m\Documents\ISS Schematics - Chas\40m\v1\ISS_v3-c-Comparator.SchDoc			Date: 8/30/2013 Time: 1:34:00 PM Sheet 4 of 5

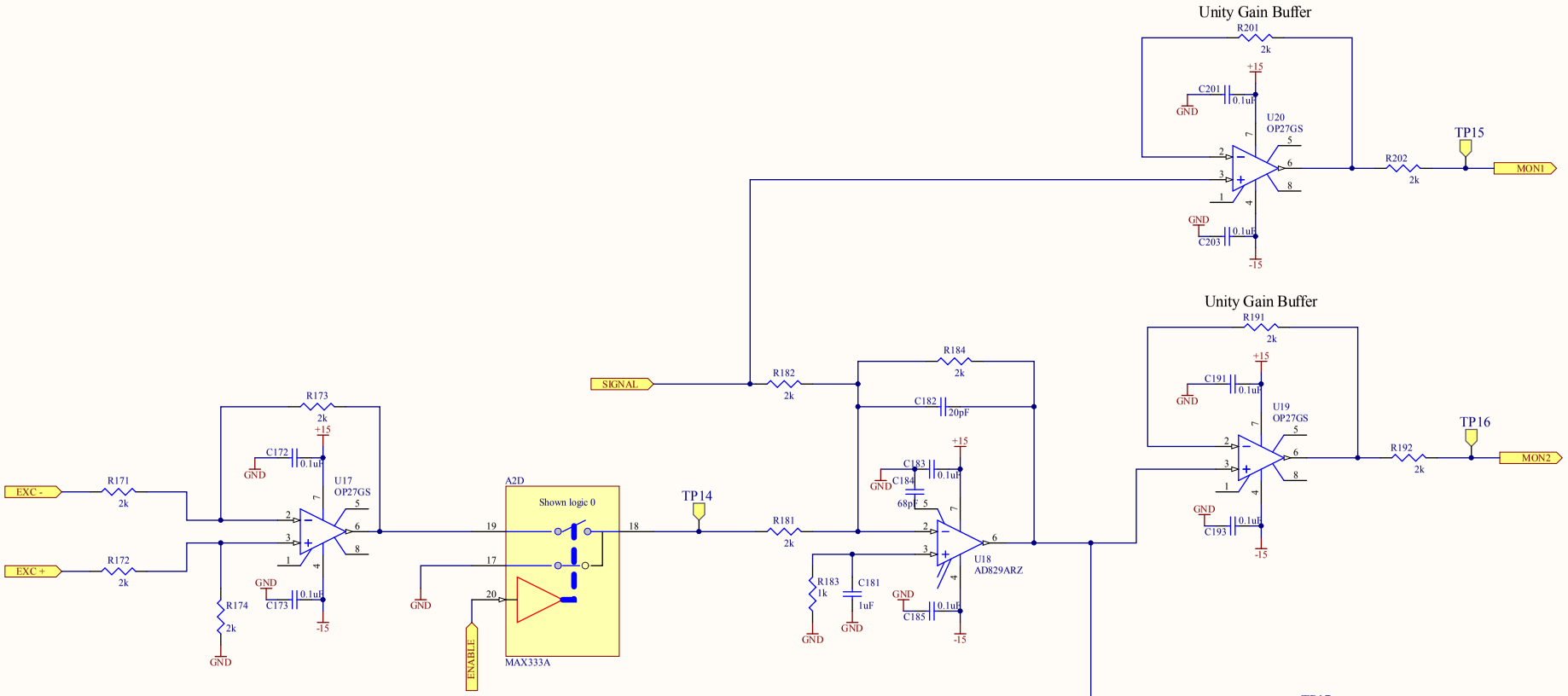

Title: *ISS: Excitation*			*LIGO Laboratory* *California Institute of Technology* *Massachusetts Institute of Technology*	LIGO
Size: B	DCC Number: *	Revision: *	Engineer: *Charles Blakemore*	Date: 8/30/2013
File: C:\Users\cit40m\Documents\ISS Schematics - Chas\40m\v1\ISS_v3-d-Excitation.SchDoc				Time: 1:34:00 PM
				Sheet 5 of 5

Last Edited:

D1300694-v1
40m/Caltech ISS Board

Serial Number